Measurement and Analytical Study of the Correlation Properties of Subchannel Fading for Noncontiguous Carrier Aggregation

Ruonan Zhang, *Member, IEEE*, Zhimeng Zhong, Yang Zhang, Stan Lu, and Lin Cai, *Senior Member, IEEE*

***Abstract*—The new multichannel/multicarrier technologies can potentially support much higher data rates in mobile multiple-access environments, such as carrier aggregation (CA) defined in the fourth-generation Long-Term Evolution Advanced enhancement. The correlation properties of noncontiguous subchannels are critical for the performance of CA, including cell coverage, frequency diversity, and channel state estimation. This paper has studied the correlation of the large-scale fading (LSF) and small-scale fading (SSF) of arbitrarily separated subchannels by realistic channel measurement and analytical modeling. We first obtain the subchannel correlation from the ultrawideband (UWB) channel measurement. This new approach avoids probing multiple subchannels simultaneously with channel sounders, which would be prohibitively complicated. The cross correlation of two distinct subchannels and the autocorrelation of a single subchannel are evaluated. Second, a new propagation model for the Nakagami-m fading in a multipath environment is proposed. The frequency-domain level crossing rate (FD-LCR) is defined and derived based on the propagation model. Then, a Markov chain for the frequency fading of the wideband channel is established, which can generate the correlated gain/power of subchannels in a wide bandwidth. Therefore, this model can be used as a fast simulator of CA over correlated subchannels. Finally, the cross correlation coefficients (CCCs) between two Nakagami-m fading subchannels obtained from the measurement and the proposed Markov model are compared with the analytical results in the literature. This paper provides important insights into the fading correlation of the multicarrier channels and can be applied to the design and simulation of indoor/outdoor multicarrier communications.**

***Index Terms*—Carrier aggregation (CA), channel measurement, channel modeling, CLEAN, fading, ultrawideband (UWB).**

Manuscript received February 8, 2013; revised July 5, 2013, October 21, 2013, and January 14, 2014; accepted February 25, 2014. Date of publication March 26, 2014; date of current version November 6, 2014. This work was supported in part by the National Natural Science Foundation of China under Grant 61202394 and Grant 61301092, by the Ministry of Education of China through the Program for New Century Excellent Talents in University of China, by Northwestern Polytechnic University (NPU) through the NPU Fundamental Research Program, by the Higher Education Doctoral Program Foundation under Grant 20116102120030, and by the Foundation for Selected Chinese Oversea Scholars. This paper was presented in part at the IEEE Global Communications Conference, Anaheim, CA, USA, December 3–7, 2012. The review of this paper was coordinated by Prof. D. B. da Costa.

R. Zhang is with the School of Electronics and Information, Northwestern Polytechnical University, Xi'an 710072, China (e-mail: rzhang@nwpu.edu.cn).

Z. Zhong and S. Lu are with Huawei Technologies Ltd., Xi'an 710065, China (e-mail: zmzhong@huawei.com; stan.x.lu@huawei.com).

Y. Zhang is with Xidian University, Xi'an 710126, China.

L. Cai is with the Department of Electrical and Computer Engineering, University of Victoria, Victoria, BC V8W 2Y2, Canada (e-mail: cai@ece.uvic.ca).

Color versions of one or more of the figures in this paper are available online at http://ieeexplore.ieee.org.

Digital Object Identifier 10.1109/TVT.2014.2314028

I. Introduction

MULTICHANNEL/MULTICARRIER technologies have recently attracted increasing interest due to their higher data rate capacity and flexibility in spectrum allocation and multiple access. For example, carrier aggregation (CA) has been proposed as an enhancement to Long Term Evolution (LTE) Advanced [1] where a terminal may combine several subchannels (e.g., with the bandwidth of 20 MHz). Because aggregating noncontiguous available subchannels is supported, CA may further exploit the frequency diversity.

Since the existence of multipath propagation gives rise to frequency-selective fading channels, the correlation between the aggregated subchannels in CA plays an important role in the performance of the multicarrier transmission. One of the potential applications of the correlation of the large-scale fading (LSF) of the subchannels is analysis of the cell coverage. We know that the capacity of one subchannel between a base station (BS) and a mobile station (MS) depends on the received SNR according to the Shannon theory, and the SNR is determined by the LSF (i.e., the path loss (PL) and shadowing). Now, the problem is if there is a significant difference between the average capacities of two separated subchannels or if is it possible to get much higher capacity when we switch from one subchannel to another. Another application is channel state estimation. The channel gain is usually estimated to perform automatic gain control at the receiver and automatic modulation and coding at the transmitter [2]. In CA, how much are the two subchannels separated such that their states are similar? Given the similarity of subchannel states, estimation of one subchannel may be sufficient, and the other estimation cost can be reduced. Furthermore, the frequency diversity gain achieved by CA also depends on the subchannel correlation. The answers to both questions depend on the correlation of the small-scale fading (SSF) between the two subchannels.

Therefore, it is important to quantify the correlation of the two subchannels that may be arbitrarily separated. In [3], Filho *et al.* derived the accurate closed-form expression for the cross correlation function (CCF) between two nonidentically distributed Nakagami-m fading processes with time, space, and/or frequency spacing. Thus, the cross correlation coefficient (CCC) can be obtained analytically. This insightful work provides a very useful theoretical study on the correlation property needed for CA. However, to the best of our knowledge, realistic measurements on the correlation, with respect to frequency spacing, have not been reported in the literature.

The key reason is that, using the traditional channel sounding technology, the sounder needs to simultaneously probe multiple subchannels, which requires prohibitively high complexity. As specified in [4], the initial identified bands for CA are nonuniformly scattered from 0.4 to 5 GHz. Elektrobit and Medav are two companies with sound reputations in channel measurement around the world. However, their state-of-the-art channel sounders, named Propsound and RUSK, respectively, cannot support simultaneous multiband probing across gigahertz spacing. This motivated us to search for an alternative approach to tackling this problem.

Furthermore, it is useful to design a multisubchannel simulator that can directly generate the correlated Nakagami-m fading subchannel states fast and easily. The finite-state Markov chain (FSMC) model, which can generate the correlated time-varying fading channel states, has been proposed and widely used in the simulation and analytical study of the traditional mobile communication systems and upper layer packet-based protocols [5]. Is it possible to establish an FSMC to generate the correlated subchannel states in the frequency domain?

In this paper, the correlation of the LSF and SSF of the subchannels is investigated from two aspects: the realistic measurement and the Markovian modeling. We consider a general multicarrier system as follows. The operator is licensed with a wideband spectrum over a couple of gigahertz, called the *operator channel*. The operator channel is divided into a number of *subchannels* (i.e., subbands) of several kilohertz or megahertz, which are assigned to different users and can be aggregated by CA. The subchannels have approximately flat fading. Our target is to quantify the correlation of the *LSF* and the *SSF* of the subchannels. The LSF refers to the shadowing effect caused by obstructors, which, for the indoor scenario, typically happens when the receiver moves from one room to another. The SSF refers to the frequency-selective fading caused by the multipath propagation.

The main contributions of this paper are twofold. First, we develop an alternative approach based on the indoor ultrawideband (UWB) channel measurement. The idea is to extract the fading information of various subchannels from the UWB channel frequency response, which is obtained by probing the channel with nanosecond-level pulses. This technique not only avoids the traditional complicated sounder implementation but is also convenient for extracting the subchannel power density with various central frequencies and bandwidths. A comprehensive study is presented, including: 1) the cross correlation of the LSF and of the SSF of two separated subchannels, and 2) the autocorrelation of the LSF and the SSF of one single subchannel.

Second, a frequency-domain FSMC (FD-FSMC) model describing the power spectrum density (PSD) is proposed, which can generate the correlated states of the subchannels sequentially. We propose a propagation model for the subchannel Nakagami-m fading process. Then, the *frequency-domain level crossing rate* (FD-LCR) for a wideband frequency-selective channel is defined and derived, based on which the transition probabilities of the FD-FSMC is determined. Finally, the CCC of two subchannels obtained from the measurement and the FD-FSMC are compared with the analytical result in [3].

The remainder of this paper is structured as follows. We briefly provide an overview the related work and the UWB channel measurement in Section II. The modified CLEAN algorithm and the process of obtaining the LSF and the SSF of the subchannels are proposed in Sections III and IV, respectively. The correlation of the spatial fading of the subchannels are evaluated in Section V based on the measurement results. The propagation model and FD-LCR of the subchannels are proposed in Section VI. Section VII presents the FSMC to evaluate the SSF correlation analytically. The analytical and measurement results are compared in Section VIII to validate the channel model. Section IX concludes this paper and indicates further research issues.

II. Related Work and Ultrawideband Propagation Measurement

A. Correlation of Two Channels With Frequency Separation

While extensive research has been carried out for the physical LTE channel measurement and modeling [6], only a handful of papers has considered the correlation between subchannels. In [7] and [8], and [9], the LSF correlation for outdoor and indoor scenarios, respectively, has been studied. Due to the limit of the channel sounders, only the correlation between several wireless links with fixed frequencies were measured. The analytical results of the CCF between nonidentical Nakagami-m fading processes with space, time, and frequency spacing were presented in [3] and [10]. The closed-form expression for CCC is [3, eq. (1)]

$$\begin{aligned} R(\tau,\, \Delta\omega) &= \left(\frac{\Omega_1}{m_1}\right)^{\frac{1}{2}} \left(\frac{\Omega_2}{m_2}\right)^{\frac{1}{2}} \left[\frac{\Gamma\left(m_1+\frac{1}{2}\right)\Gamma\left(m_2+\frac{1}{2}\right)}{\Gamma(m_1)\Gamma(m_2)}\right] \\ &\quad \times {}_2F_1\left(-\frac{1}{2},\, -\frac{1}{2};\, m_2;\, \rho\right) \\ &\approx \sqrt{\frac{m_1}{m_2}}\rho(\tau,\, \Delta\omega) \end{aligned} \tag{1}$$

where Ω_1 and Ω_2 are the average power values of the Nakagami-m fading processes, $\Gamma(\cdot)$ is the gamma function, and ${}_2F_1(\cdot,\cdot;\cdot;\cdot)$ is the hypergeometric function. In (1), ρ is the autocorrelation coefficient of the underlying Gaussian random components [11]. To consider two fading instances with the time and frequency separation of τ and $\Delta\omega$ (in radians per second) received on one omnidirectional antenna, we have [3, eq. (5)]

$$\rho(\tau,\, \Delta\omega) = \frac{J_0^2(\omega_D\tau)}{1+(\Delta\omega\bar{T})^2} \tag{2}$$

where $\omega_D = 2\pi f_D$ is the maximum Doppler shift in radians per second, $J_0^2(\cdot)$ is the Bessel function of the first kind and zeroth order, and $\bar{T}$ is the mean excess delay of the scattered waves. The analytical works in [3] and [11] are very insightful as they derived the unified closed-form expression for the generic-order CCF of two Nakagami-m fading instances with arbitrary temporal, frequency, and spatial separation. However, the practical measurement of the subchannel correlation with frequency separation is still rarely reported in the literature.

On the other hand, to conduct analysis and simulation of communication systems and upper layer protocols taking into account the correlated variation of wireless channels, a simple stochastic channel model is very useful. The FSMC model has been proposed to describe the temporal variation of single or even diversity-combined Rayleigh and Nakagami-m fading processes [5], [12]. Because these models can generate the correlated channel states for discrete time instances (e.g., every packet transmission interval) and can be also easily incorporated into the packet-level analysis frameworks of upper layer protocols, they have been widely used in the simulation and analysis of traditional narrow-band systems. The time-domain FSMCs are established based on the higher order statistics, i.e., LCR, of the fading channel. Establishing the FSMC model for the frequency-selective fading between subchannels with appropriate correlation motivates the work in this paper.

Following the previous approach, it is critical to determine the FD-LCR between the gain/power of subchannels. In the early work of [13], the LCR of the channel's transfer function was investigated from the Fourier transform of the power delay profile (PDP) model for the frequency-selective Rician fading channel. In [14], the channel gain LCR between adjacent subchannels in orthogonal frequency-division multiplexing (OFDM) systems was obtained based on the Jakes' model. In [15], a novel general framework to calculate the LCR and the average fade duration (AFD) of a sampled fading channel was presented. The authors applied the method to the frequency response envelope in an OFDM system. In this paper, we extend the work in [14] for a general wideband radio channel. Furthermore, the CCC between two subchannels in the developed FSMC is compared with both the measurement and analytical results [3], [10]. The objective of this paper is to provide a fast simulator to support the wideband channel modeling and design of multicarrier communications such as CA.

B. UWB Channel Measurement

The characterization of the subchannel correlation in this paper is based on the UWB propagation measurement performed in a typical modern office building [16]. The measurement is briefly reviewed for convenience. The placement of the transmitter and 14 receiving regions are shown on the floor plan in Fig. 1(a). In each region, the receiver antenna was placed at 49 positions arranged spatially on a 7 × 7 square grid with 15-cm spacing, as shown in Fig. 1(b). The point on the ith row and jth column on the grid is indexed as (i, j). As a convention, the first row is always parallel and adjacent to the north wall of the room.

The two diamond-dipole UWB antennas are vertically polarized and nearly circularly symmetric about their vertical axes [18]. The pulser at the transmitter generates Gaussian-shaped pulses with 2-ns duration periodically to probe the channel. The response waveform is recorded by a digital sampling oscilloscope for a 300-ns time window. Since the antennas and other processing apparatus may differentiate and filter the pulser's output due to their implicit bandlimiting and frequency-selective effect, the received pulses may be severely distorted. Fig. 2(a) shows the three reference waveforms recorded with 1-m transceiver separation and the receive antenna rotated by 0°, 45°, and 90°, respectively. According to the environment, the earliest multipath component (MPC) reflected from scatterers arrives about 4 ns after the line-of-sight (LOS) signal. Thus, Fig. 2(a) represents the *clean pulses* propagated via the LOS path without being corrupted by the MPCs, which embody the characteristics of the pulse driver and the antenna systems.

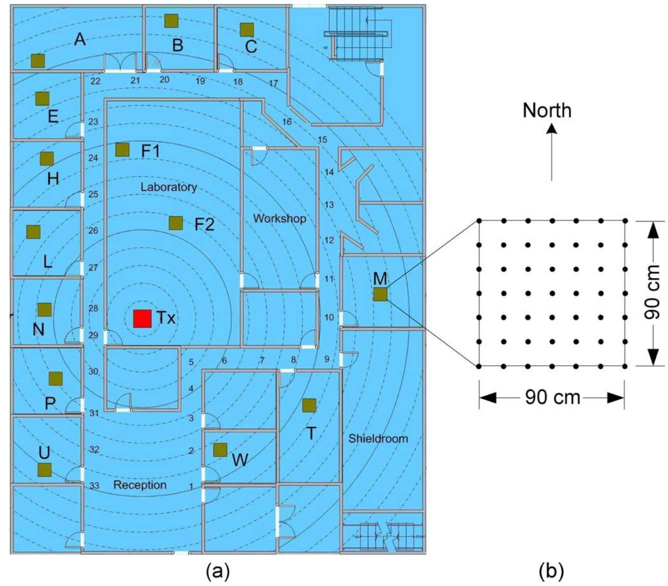

Fig. 1. Floor plan of the office building and the measurement grid [17]. (a) Building floor plan. (b) Measurement grid.

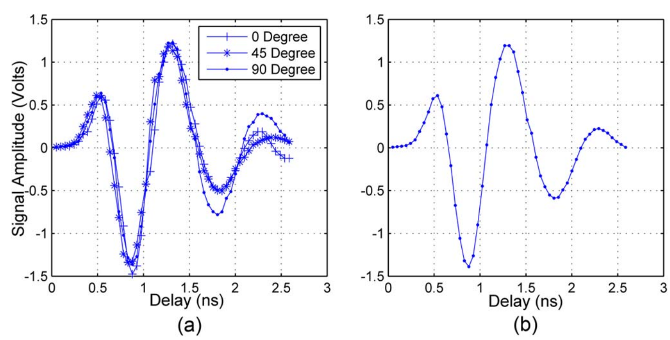

Fig. 2. Received clean pulses at 1-m separation distance and pulse template. (a) Measured in three angles. (b) Averaged and power normalized.

Substantial variation in the SNR of the recorded waveforms at different locations is observed. The SNR in the offices close to the edge of the building is much lower, due to large PL and external radio inferences. Therefore, the measurement results in rooms B and C are excluded from the following analysis.

III. CLEAN Algorithm and Channel Impulse Response Extraction

The approach to identifying the fading of subchannels from the UWB propagation measurements includes three steps. We first extract the UWB CIRs from each individual measurement, using a modified CLEAN algorithm [19]. Then, the frequency response and the PSD are obtained by performing Fourier transform of the channel impulse responses (CIRs). Finally, the power of subbands is acquired by integrating the PSD over the corresponding bandwidth.

A. Modified CLEAN Algorithm

The impulse response of the multipath channels is often modeled as the summation of discernible paths with different time delays, amplitude attenuation, and phase shift, expressed by

$$h(t) = \sum_{n}^{N} a_n \delta(t - \tau_n) \tag{3}$$

where a_n and τ_n are the complex magnitude and delay of the nth propagation path, respectively. When probing the channel with short pulses, as previously mentioned, the received waveform is a bandlimited and distorted form of the pulses driving the transmitter's antenna, which is denoted $\tilde{p}(t)$. A typical multipath model for the observed response, which is denoted $r(t)$, is

$$r(t) = \sum_{n}^{N} a_n \tilde{p}(t - \tau_n). \tag{4}$$

If $\tilde{p}(t)$ is known, deconvolution techniques can resolve a_n and τ_n such that a continuous-time CIR, which is denoted $\hat{h}(t)$, can be extracted from the measured waveform.

A simple deconvolution technique involves the inverse filtering. The channel transfer function can be estimated by $\hat{H}(\omega) = R(\omega)/P(\omega)$, where $R(\omega)$ and $P(\omega)$ are the Fourier transforms of $r(t)$ and $\tilde{p}(t)$, respectively. However, this approach is susceptible to high noise levels, which may generate several near-coincidental and opposing taps from a single impulse plus noise [20]. Another technique is the CLEAN algorithm, which is initially used to enhance radio-astronomical images [21] and has been applied to UWB channel characterization [20], [22]. The CLEAN algorithm performs subtractive deconvolution, identifying impulses directly from the waveform; therefore, this approach is less prone to noise. However, different from the original CLEAN algorithm for astronomical image processing, we need to decide the propagation paths for CIR extraction. Setting the threshold for recognizing paths is nontrivial. This is mainly because, in the practical measurement, the distance between the transceivers changes significantly, resulting in the large variation of the power of the captured signal. If the threshold is too low, many pseudopaths may be identified, whereas if it is too high, some true paths can be missed. Since Win's set of measurement data shows substantial variation in the noise power, adopting a fixed threshold may not be suitable. Motivated by this fact, we propose adjusting the threshold for each measurement snapshot adaptively according to the noise level.

We take the average of the three clean pulses in Fig. 2(a) and use the waveform from 4.73 to 7.56 ns as the final clean pulse, as plotted in Fig. 2(b) (the x-axes have been reset to start from 0). The clean pulse is denoted $\bar{p}(t)$. Furthermore, to obtain the amplitude (or energy) of the impulses in the CIR, the energy of $\bar{p}(t)$ is normalized by

$$\tilde{p}(t) = \frac{\bar{p}(t)}{\int_{o}^{T} \bar{p}^2(t) dt} \tag{5}$$

where T is the pulse duration. $\tilde{p}(t)$ is used as the template pulse in the deconvolution.

The proposed deconvolution approach is performed by the steps in Algorithm 1.

Algorithm 1 Iteration Steps of modified CLEAN Algorithm

Require: $r(t)$: captured waveform, $\tilde{p}(t)$: pulse template, T_w: duration of $r(t)$, T_n: duration of the noise waveform;
Ensure: $\hat{h}(t)$: estimated CIR;
1: $n(t) = r(t + T_w - T_n),\ t \in [0,\ T_n]$;
2: $\Upsilon(\tau) = \int_{\tau}^{\tau+T} n(t)\tilde{p}(t-\tau)dt$;
3: Set γ_0 such that $\mathrm{cdf}_{\Upsilon}(\gamma_0) = 90\%$;
4: $d(t) = r(t),\ t \in [0,\ T_w - T_n]$;
5: $c(t) = 0$ and $\Phi = \{\ \}$;
6: $\Gamma(\tau) = \int_{\tau}^{\tau+T} d(t)\tilde{p}(t-\tau)dt$;
7: $\tau_M = \arg\max_{\tau}\{|\Gamma(\tau)|\}$ and $\gamma_M = \Gamma(\tau_M)$;
8: **while** $\gamma_M >= \gamma_0$ and $\tau_M ! \in \Phi$ **do**
9: $\quad \Phi = \Phi \cup \{\tau_M\}$;
10: $\quad c(t) = c(t) + \gamma_M \delta(t - \tau_M)$;
11: $\quad d(t) = d(t) - \gamma_M \tilde{p}(t - \tau_M)$;
12: $\quad \Gamma(\tau) = \int_{\tau}^{\tau+T} d(t)\tilde{p}(t-\tau)dt$;
13: $\quad \tau_M = \arg\max_{\tau}\{|\Gamma(\tau)|\}$ and $\gamma_M = \Gamma(\tau_M)$;
14: **end while**
15: $\hat{h}(t) = c(t) = \sum \gamma_M^{(i)} \delta(t - \tau_M^{(i)})$

The first three steps determine an appropriate power threshold, which is used to distinguish if the correlation is $\tilde{p}(t)$ with a received pulse through a propagation path or with the background noise in the following steps. By observing the captured channel responses with the duration of $T_w = 299.8$ ns in all the measurements, the excess delay is no more than 250 ns. Thus, the last 50-ns waveform is just background noise and is used to estimate the range of the correlation coefficient of $\tilde{p}(t)$ with noise. Therefore, step 1 extracts the last $T_n = 50$ ns waveform from the captured signal as the noise. By calculating the correlation coefficient function, step 2 gives a sample set of the correlation results of the template pulse $\tilde{p}(t)$ and the background noise for a certain measurement point. Step 3 sets the decision threshold as γ_0, which is the 90th percentile of the distribution of $\Upsilon(\tau)$. Consequently, if the correlation coefficient of a waveform and $\tilde{p}(t)$ is smaller than γ_0, the waveform is quite likely just background noise. Otherwise, we regard that the waveform contains a copy of the signal and then extract the gain of the path in the following steps.

Step 4 sets the dirty map by the captured waveform with the noise sequence of $n(t)$ removed. Step 5 initializes the clean map $c(t)$ and the path delay set Φ, respectively. Step 6 forms the correlation function of the dirty map $d(t)$ and the template $\tilde{p}(t)$, which would peak at the delays of the MPCs. Then, we obtain the delay and the corresponding polarized power of the maximal amplitude of $\Gamma(\tau)$ by step 7, where $|\cdot|$ takes the absolute value. Steps 9–13 perform the iteration of the CLEAN algorithm to extract the path information. Once a path is identified by checking the correlation function, the set Φ and the clean map c_t are updated by adding the delay and the corresponding impulse in steps 9 and 10, respectively. The dirty map is then cleaned by subtracting the scaled and delayed

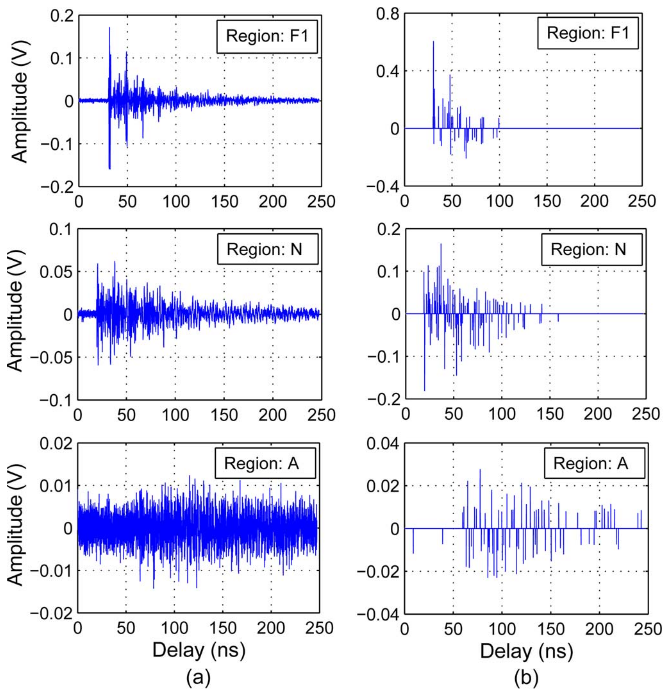

Fig. 3. Received waveforms and extracted CIRs. (a) Received waveform. (b) CIR.

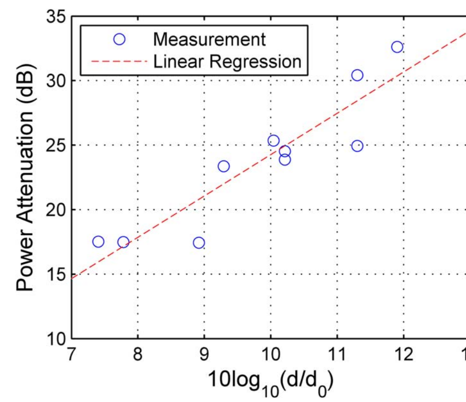

Fig. 4. Power attenuation in 2–6 GHz of SSA-PSD versus logarithm distance.

template pulse in step 11. Steps 12 and 13 are the same as steps 6 and 7 but are performed iteratively inside the loop. If the stopping criteria in the WHILE statement is not satisfied, i.e., even the correlation function peak is produced by the correlation with noise or has already occurred in the previous iterations, the iteration finishes, and the estimated valid paths have all been identified.

Finally, the CIR extracted from $r(t)$ is organized in step 15, where $\gamma_M^{(i)}$ and $\tau_M^{(i)}$ are the recorded correlation function peaks and the corresponding delays in the iterations. In summary, the algorithm above is designed to adapt to the substantially varying noise floor and is simple to implement, which is suitable for processing the indoor UWB channel measurements.

B. Extracted CIRs of Typical Scenarios

The extracted CIRs of some typical scenarios using the CLEAN algorithm are demonstrated in Fig. 3, where the original waveforms are recorded at the center positions of three regions. Regions $F1$, N, and A are representative for the LOS, non-LOS (NLOS) with high SNR, and NLOS with low SNR scenarios (longer propagation distance and more obstructors), respectively. It can be seen that the multipath profiles have an obvious cluster-arriving and double exponentially decaying pattern. Note that the signal magnitude for NLOS is attenuated significantly.

The time resolution of the CLEAN algorithm is equal to the width of the main lobe of the autocorrelation function of the template pulse. The narrower the autocorrelation function is, the higher the time resolution of the extracted CIR. Hence, the UWB probing pulse makes it possible to characterize the channel frequency response within a high bandwidth.

IV. Finding Subchannel Fading

In most of the existing channel models, the propagation loss is presented by the product of the PL, LSF, and SSF. Furthermore, due to the frequency-dependent propagation effects, the loss is a function of frequency and of distance.

We are interested in the total bandwidth of 2–6 GHz, and the bandwidth of one subchannel is 20 MHz. The received power of the subchannels and that of the frequency-dependent fading are investigated based on the PSD, which is $\hat{G}(f) = |\hat{H}(f)|^2$, where $\hat{H}(f)$ is the channel frequency response obtained by the Fourier transform of $\hat{h}(t)$. Then, the received power of a subchannel is acquired by integrating $\hat{G}(f)$ over the corresponding bandwidth [19].

A. Averaging SSF Within Measurement Regions

PL and SSF should be removed from the received power attenuation to estimate the LSF of the subchannels. As previously mentioned, the SSF for this indoor UWB channel measurement is introduced when the receiver moves over the region grid within a room.

We refer to the PSD obtained at a grid point as the *individual PSD*, whereas the PSD averaged over the 49 positions within one region is denoted as the *SSF spatial-averaged PSD* (SSA-PSD). The center frequency of our bandwidth of interest is 4 GHz; therefore, the grid edge of 90-cm length is approximately of 10λ, which is proposed as a good window size to average out SSF without distorting the LSF patterns for indoor multipath propagation [9], [23]. Then, the LSF may be investigated by analyzing the variation of the SSA-PSDs over different regions (i.e., rooms).

B. Extracting the PL Within Interested Bandwidth

By integrating the SSA-PSD over the 2–6 GHz bandwidth, we obtain the average total energy of each region, which is denoted $\bar{P}_X$ where X represents the alphabet of the region (e.g., X is $F1$, A, E, etc.). The total energy of the reference measurement (with a separation distance of $d_0 = 1$ m) can be acquired in the same way, which is denoted P_0. Then, the power attenuation for region X can be defined as $\bar{A}_X = P_0/\bar{P}_X$. As suggested by the scatter plot in Fig. 4, we obtain the linear regression of the measured power attenuation (in decibels) as a function of the logarithm of the transceiver distance. The PL model of the empirical attenuation is

$$\mathrm{PL}(d)_{\mathrm{dB}} = 10\log_{10}\left(\frac{P_0}{\bar{\bar{P}}(d)}\right) = 32.02\log_{10}\left(\frac{d}{d_0}\right) - 7.75 \tag{6}$$

where $\bar{\bar{P}}(d)$ is the expected received power averaged over both the LSF and SSF at distance d.

C. Finding the Subchannel LSF and SSF

Because we are interested in the correlation of the subchannel LSF (i.e., the average power variation), for easy calculation, we approximate that all the subchannels have the same PL exponent. In other words, the slope of the linear PL model (in decibels) is the same within the total bandwidth of interest. This approximation does not affect the evaluation of LSF correlation because we are interested in the variation of the power attenuation.

As previously mentioned, there are a total of 200 subchannels inside the bandwidth of 2–6 GHz. Suppose that the received power of the kth subchannel in the reference measurement is $P_0^{(k)}$. Thus, the expected received power for the subchannel at a measurement region is $\bar{\bar{P}}_X^{(k)} = P_0^{(k)}/\mathrm{PL}(d_X)$, where $\mathrm{PL}(d_X)$ is obtained from (6). The SSF-averaged received power of the subchannel is obtained by integrating the SSA-PSD over the subchannel bandwidth, which is denoted $\bar{P}_X^{(k)}$. Then, the LSF of the subchannel is $Y_X^{(k)} = \bar{\bar{P}}_X^{(k)} - \bar{P}_X^{(k)}$.

The small-scale statistics are derived by considering the deviations of the 49 local PSDs from the SSA-PSD. The received power of the kth subchannel at the measurement position (i, j), which is denoted $P_{X,ij}^{(k)}$, is obtained by integrating the local PSD over the bandwidth. Hence, the SSF is $Z_{X,ij}^{(k)} = \bar{P}_X^{(k)} - P_{X,ij}^{(k)}$.

V. Correlation of the Subchannel Fading

The study of the spatial variation of the subchannels includes two aspects [19]: 1) the cross correlation of the LSF and SSF of two different subchannels, and 2) the autocorrelation of the LSF and the SSF of one single subchannel.

A. Cross Correlation of the LSF of Two Subchannels

The LSFs of the kth and lth subchannels are denoted by the random variables (RVs) $Y_{\mathrm{sub}}^{(k)}$ and $Y_{\mathrm{sub}}^{(l)}$, respectively. The measured LSFs obtained from the SSA-PSDs of the ten NLOS regions are the samples of the two RVs (as previously mentioned, regions B and C are excluded due to very high noise floor). Then, the CCC can be calculated as follows:

$$\rho_{k,l} = \frac{\mathrm{cov}\left(Y_{\mathrm{sub}}^{(k)}, Y_{\mathrm{sub}}^{(l)}\right)}{\sqrt{\mathrm{var}\left(Y_{\mathrm{sub}}^{(k)}\right)\mathrm{var}\left(Y_{\mathrm{sub}}^{(l)}\right)}} \tag{7}$$

where $\mathrm{cov}(\cdot)$ and $\mathrm{var}(\cdot)$ are the covariance and variance of the given RV(s), respectively.

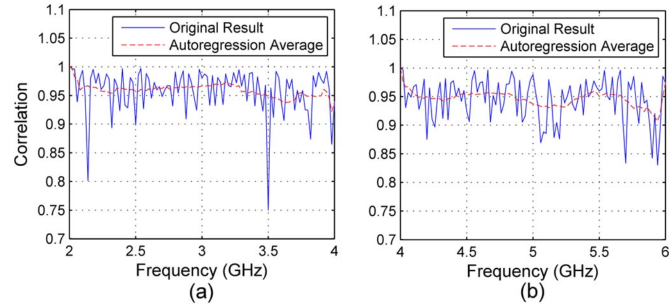

Fig. 5. CCC of the LSF of two subchannels.

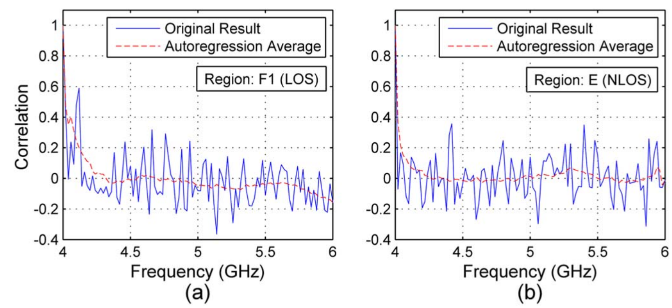

Fig. 6. CCC of the SSF of two subchannels.

Fig. 5(a) shows $\rho_{k,l}$ when the bandwidth of both subchannels is 20 MHz, the lower bound frequency of one subchannel is fixed at 2 GHz, and that of the other increases from 2 to 3.98 GHz. Thus, the separation of them increases from 0 to almost 2 GHz. Fig. 5(b) shows a similar case, but the lower bound frequency of one subchannel is fixed at 4 GHz and that of the other changes from 4 to 5.98 GHz. Furthermore, the autoregression of the measurement results averaged by a sliding window with the size of 20 is also plotted by the dashed lines, to remove the random fluctuation of the measurements.

As shown, the LSF of two subchannels is close to full correlation, with the correlation coefficient mostly larger than 0.9. This is not surprising because the shadowing effect caused by obstructors should be consistent for the subchannels inside the bandwidth of interest. Furthermore, comparison of the two subfigures also illustrate that the averaged correlation coefficient is always about 0.95, independent from the frequency separation and the central frequencies.

B. Cross Correlation of the SSF of Two Subchannels

When the receiver moves over a measurement region grid, the SSF of a subchannel (i.e., the difference of the received power obtained at a position and that of the SSA-PSD) is an RV. The SSF of the kth and lth subchannels are denoted by the two RVs $Z_{\mathrm{sub}}^{(k)}$ and $Z_{\mathrm{sub}}^{(l)}$, respectively. For a given region, the measured SSF of the two subchannels at the grid points $Z_{X,ij}^{(k)}$ and $Z_{X,ij}^{(l)}$ can be regarded as the 49 observations of $Z_{\mathrm{sub}}^{(k)}$ and $Z_{\mathrm{sub}}^{(l)}$, respectively. Then, the CCC is calculated similarly according to (7).

Fig. 6 shows $\rho_{k,l}$ of two regions, $F1$ (LOS scenario) and E (NLOS scenario), presented in the same way as in Fig. 5(b). It is observed that the correlation reduces quickly with the increase in the separation of the two subchannels. The decorrelation

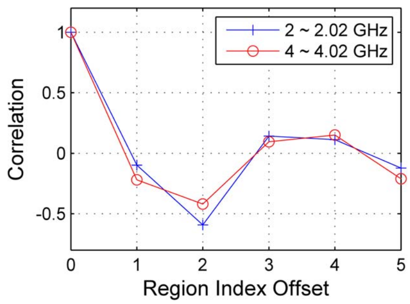

Fig. 7. Autocorrelation coefficient of the LSF of a single subchannel.

distance is less than 100 MHz, by which the coefficient has dropped to below 0.2. One possible explanation is that the intensive multipath effect in an indoor environment results in severe superimposition of the MPCs at the receiver. With a small change in the frequency, the in-phase enhancement and out-of-phase cancelation will vary dramatically. Thus, the SSF is quite sensitive to the carrier frequency. In addition, we can see that the correlation coefficient of the LOS scenario is slightly larger than that of the NLOS scenario. This is expected since the LOS component does not have the superimposition effect and hence remains consistent for frequency change.

C. Autocorrelation of the LSF of a Subchannel

The autocorrelation of the LSF refers to a single subchannel for the NLOS scenario. The measured LSF of the kth subchannel $Y_X^{(k)}$ obtained from the SSA-PSD of the ten NLOS regions can be regarded as a random sequence. The autocorrelation of the sequence can be calculated. The results of two representative subchannels, i.e., 2–2.02 and 4–4.02 GHz, are shown in Fig. 7. The x-axis is the index of the measurement regions, which are reordered such that the distance to the transmitter is increasing.

As shown, the LSF of a single subchannel is almost uncorrelated for different rooms. This is expected because the shadowing effect is mostly specific to the surrounding environment. Similar results were observed in [9], where the decorrelation distance for the LSF of an indoor wireless link is on the order of 1–2 m.

D. Autocorrelation of the SSF of a Subchannel

The autocorrelation of the SSF of one subchannel can be treated in the same way as earlier in the frequency domain. However, since the autocorrelation actually depends on the variation of the CIR for the movement of the receiver within a small distance (such as several wavelengths), the variation of the PDP in the time domain reflects the variation of the power of subchannels. Therefore, we choose to directly study the autocorrelation of PDP here. In this way, we can also see how the wideband CIR changes in the time domain.

The measured PDPs at all positions in a region are aligned and quantized. First, each local PDP is aligned by an appropriate delay reference, removing the background noise before the arrival of the true response signal in the recorded waveform. As in [17], we take the reference delay as the absolute propagation

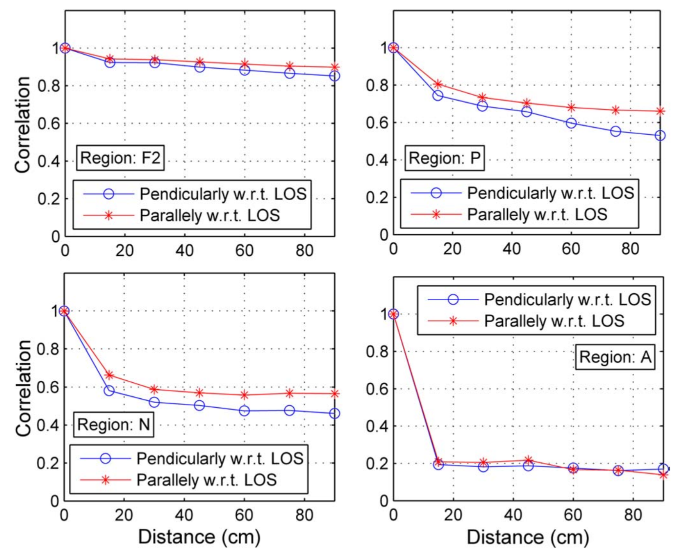

Fig. 8. Autocorrelation coefficient of the SSF of TDL-PDPs.

time of the direct path between the transceivers: $\tau_{\mathrm{Ref}} = d/c$, where d is the transceiver distance, and c is the speed of light. Second, the delay axis is quantized into bins with a bin width of $\Delta\tau = 2$ ns, and the received power within each bin is integrated to obtain the tapped delay line (TDL) form. The TDL-PDP at the position of $(i,\, j)$ is denoted $G^{(ij)}(n)$, where n is the index of the bins.

We consider two cases. First, the receiver moves in the direction perpendicular to the LOS path. The method to calculate the correlation coefficient of the PDPs before and after the receiver moves by k grid blocks is as follows. If the direction of the movement is from west to east (i.e., along the row direction of the grid, e.g., in the regions of A, U, etc.), we fist concatenate the PDPs $G^{(ij)}$, where $i = 1, 2, \ldots, 7$ and $j = 1, 2, \ldots, 7 - k$, together to form a sequence. Then, the PDPs $G^{(ij)}$, where $i = 1, 2, \ldots, 7$ and $j = k + 1, k + 2, \ldots, 7$, are concatenated as another sequence. The correlation coefficient of the two sequences is calculated. The number of movement steps could be $k = 0, 1, \ldots, 6$. The second case is that the receiver moves in the direction parallel to the LOS path, and the coefficients are analyzed in the same way.

The results for four typical propagation environments are plotted in Fig. 8. The PDPs are much less correlated in the NLOS scenarios than in the LOS scenario. This is perhaps because the LOS component makes the most significant contribution to the PDP, and it remains stable when the receiver moves over a couple of wavelengths without significant change in the environment. Furthermore, the correlation becomes smaller with the decrease in SNR, indicating that the PDP varies faster and more significantly, e.g., in Region A where the SNR is lowest. This may be because, in such scenarios, the MPCs mostly experiences many reflections and have similar contributions to the PDP. A small movement of the receiver may lead to a large variation of the significant MPCs. Another interesting observation is that the correlation is higher when the receiver moves in parallel with the LOS path in all regions, which means that the PDP would generally vary more slowly when moving toward or backward from the transmitter.

VI. Fading Model of Subchannels

Inspired by the measurement results in Section V, we propose an FSMC model to describe the correlation of the SSF of two separated subchannels here. We consider a *static multipath* propagation channel, where there are a number of scatterers around. Suppose that the PDP of the wideband operator channel has exponentially decaying pattern, as shown in Fig. 3. The narrow-band subchannels is modeled by Nakagami-m fading, which is more general and suitable for indoor environments than the Rayleigh distribution. The simulation results obtained of the model will be compared with the measurement results in Section VIII.

A. Average PDP of Wideband Operator Channel

Typically, the exponentially decaying PDP can be expressed as

$$P(\tau) = A\exp\left(-\frac{\tau}{\tau_{\mathrm{RMS}}}\right) \tag{8}$$

where τ is the excess delay, τ_{RMS} is the RMS delay spread, and A is the maximum received power at $\tau = 0$ (i.e., the first arrived MPC). Since the physical propagation environments are random, (8) can be regarded as the average PDP of the multipath channels.

We consider the *valid MPCs* whose received power (i.e., the square of the channel gain) is above the threshold, which is defined as αA, where α is the threshold coefficient (e.g., $\alpha = 0.1$). Therefore, the maximal excess delay of the valid MPCs is

$$\tau_M = -\tau_{\mathrm{RMS}} \cdot \ln\alpha. \tag{9}$$

B. Multipath Propagation Model of Subchannels

The bandwidth of a subchannel for one user is denoted B_s. The CIR of a narrow-band subchannel is the superposition of the MPCs, which results in the flat fading. Suppose there are N valid MPCs and the excess delay and power of the jth MPC are τ_j and $P(\tau_j)$, respectively. Without loss of generality, we assume that τ_j is uniformly distributed from 0 to τ_M, i.e., $\tau_j \sim U[0,\ \tau_M]$, where τ_M is defined as in (9). Thus, the received signal of a subchannel, which is the superposition of the MPCs, can be expressed as

$$\begin{cases} x(f_c) = \sum_{j=1}^{N} a_j\ \cos(2\pi\tau_j f_c + \theta_j) \\ y(f_c) = \sum_{j=1}^{N} a_j\ \sin(2\pi\tau_j f_c + \theta_j) \end{cases} \tag{10}$$

where f_c is the carrier frequency of the subchannel, and $x(f_c)$ and $y(f_c)$ are the superposition of the in-phase and quadrature components of the N paths, respectively. θ_j is the random phase shift caused by the reflection and/or diffraction on the jth path and is approximated by uniform distribution $\theta_j \sim U[0,\ 2\pi)$. a_j is the signal amplitude of the jth path, and its expectation is

$$E[a_j] = \sqrt{P(\tau_j)} = \sqrt{A\exp\left(-\frac{\tau_j}{\tau_{\mathrm{RMS}}}\right)}. \tag{11}$$

The number of paths N is usually large enough so that $x(f_c)$ and $y(f_c)$ can be considered being normally distributed due to the central limit theorem. By derivation, we can get $E[x(f_c)] = E[y(f_c)] = 0$ and

$$E\left[x^2(f_c)\right] = E\left[y^2(f_c)\right] = \frac{1}{2}\sum_{j=1}^{N} E\left[a_j^2\right] = \frac{NA(\alpha-1)}{2\ln\alpha} \tag{12}$$

where A and α are defined earlier for the wideband operator channel. Thus, $x(f_c)$ and $y(f_c)$ have the same distribution of $N(0, \sigma_{xy})$, where $\sigma_{xy} = \sqrt{(NA(\alpha-1)/2\ln\alpha)}$.

As proved in [24], the received power of the Nakagami-m fading signal is the sum of the squares of m independent Rayleigh fading signals or $2m$ independent normally distributed in-phase and quadrature signal components. Following the idea, the received signal envelope of a subchannel, which is denoted $r_s(f_c)$, is assumed to have the general Nakagami-m fading and is obtained as (for easy presentation, the independent variable f_c is ignored)

$$r_s(f_c) = \begin{cases} \sqrt{x_0^2 + \sum\limits_{i=1}^{m-1/2}(x_i^2 + y_i^2)}, & m\text{: half of integers} \\ \sqrt{\sum\limits_{i=1}^{m}(x_i^2 + y_i^2)}, & m\text{: an integer} \end{cases} \tag{13}$$

where the parameter m represents the severity of the fading, and x_i and y_i are given in (10). $r_s(f_c)$ varies randomly for different subchannels with the center frequency f_c. It is verified (in Section VIII) that $r_s(f_c)$ has Nakagami-m distribution. The probability distribution function (pdf) is

$$f_{r_s}(r) = \frac{2}{\Gamma(m)}\left(\frac{m}{\Omega_s}\right) r^{2m-1}\exp\left(-\frac{m}{\Omega_s}r^2\right) \tag{14}$$

where $\Gamma(x) = \int_0^\infty e^{-t}t^{x-1}dt$ is the gamma function, and $\Omega_s = E[r_s^2]$ is the average power of the received signal. For both cases of m being an integer or half plus an integer, we can acquire

$$\Omega_s = E\left[r_s^2\right] = \frac{mNA(\alpha-1)}{\ln\alpha}. \tag{15}$$

We have established the Nakagami-m fading model for a subchannel based on the time-spread exponentially decaying PDP of the wideband operator channel.

C. Frequency-Domain LCR

In the frequency-selective wideband operator channel, the coherence bandwidth B_c is inversely proportional to τ_{RMS}. The subchannels inside the coherence bandwidth are correlated. To evaluate the correlation of the SSF of the subchannels, we introduce the LCR of the PSD in the frequency domain [14], which is called *PSD-LCR*. The PSD-LCR refers to the average number of times the PSD crossing a given power level in the positive (or negative) direction inside a unit bandwidth. Without the loss of generality, we select the unit bandwidth as $U_f = 100$ MHz. To reach our goal, we first derived the LCR of the amplitude of the frequency response (called *FR-LCR*) as follows.

The carrier frequency of the subchannels is normalized by the unit bandwidth as $f = f_c/U_f$. The signals presented in (10) can be rewritten using the normalized frequency f. The derivatives of $x(f)$ and $y(f)$ with respect to f, which are denoted $\dot{x}(f)$ and $\dot{y}(f)$, can be obtained as

$$\begin{cases} \dot{x}(f) = -2\pi U_f \sum_{j=1}^{N} a_j \tau_j \sin(2\pi\tau_j U_f f + \theta_j) \\ \dot{y}(f) = 2\pi U_f \sum_{j=1}^{N} a_j \tau_j \cos(2\pi\tau_j U_f f + \theta_j). \end{cases} \tag{16}$$

According to the central limit theorem, $\dot{x}(f)$ and $\dot{y}(f)$ have normal distribution with the mean of 0 and the same variance of

$$\begin{aligned} \sigma_{\dot{x}\dot{y}}^2 &= E[\dot{x}^2] = E[\dot{y}^2] = 2\pi^2 U_f^2 \sum_{j=1}^{N} E\left[a_j^2 \tau_j^2\right] \\ &= 2\pi^2 U_f^2 N A \tau_{\mathrm{RMS}}^2 \frac{(\ln\alpha - 1)^2\alpha + \alpha - 2}{\ln\alpha}. \end{aligned} \tag{17}$$

Note that because the in-phase and quadrature components $x(f)$ and $y(f)$ are orthogonal, the frequency increment of Δf for the envelope r_s is equivalently $\Delta f/\sqrt{2}$ for $x(f)$ and $y(f)$. Thus, from the point of view of r_s, the derivative of the two components are $\dot{x}'(f) = \dot{x}(f)/\sqrt{2}$ and $\dot{y}'(f) = \dot{y}(f)/\sqrt{2}$, respectively. Thus, the derivative of r_s with respect to f can be derived as (if m is an integer)

$$\dot{r}_s(f) = \sum_{i=1}^{m} \frac{x_i}{r_s}\dot{x}_i' + \sum_{i=1}^{m} \frac{y_i}{r_s}\dot{y}_i' = \frac{1}{\sqrt{2}r_s}\left[\sum_{i=1}^{m} x_i\dot{x}_i + \sum_{i=1}^{m} y_i\dot{y}_i\right]. \tag{18}$$

Given the received signals x_i and y_i, $\dot{r}_s$ is the summation of a set of normal distributed RVs; therefore, $\dot{r}_s$ is normal distributed with zero mean and variance of

$$\begin{aligned} \sigma_{\dot{r}_s} &= \frac{1}{2r_s^2}\left[\sum_{i=1}^{m} x_i^2\sigma_{\dot{x}\dot{y}}^2 + \sum_{i=1}^{m} y_i^2\sigma_{\dot{x}\dot{y}}^2\right] \\ &= \frac{\sum_{i=1}^{m} x_i^2 + \sum_{i=1}^{m} y_i^2}{2r_s^2}\sigma_{\dot{x}\dot{y}}^2 = \frac{\sigma_{\dot{x}\dot{y}}^2}{2}. \end{aligned} \tag{19}$$

The derivative $\dot{r}_s$ for the case of m being the half plus an integer can be derived similarly, and the same results are obtained. Thus, the conditional pdf of the frequency derivative $\dot{r}_s$ given the signal envelope r_s is

$$f(\dot{r}_s|r_s) = \frac{1}{\sqrt{2\pi}\sigma_{\dot{r}_s}} \exp\left(-\frac{\dot{r}_s^2}{2\sigma_{\dot{r}_s}}\right). \tag{20}$$

Equation (20) shows that $\dot{r}_s$ is actually independent of r_s; hence, $f(\dot{r}_s, r_s) = f(\dot{r}_s) \times f(r_s)$.

The LCR for crossing a given envelope threshold in the positive direction is defined by $\lambda_R = \int_0^\infty \dot{r} f(\dot{r}, r = R)d\dot{r}$, where r and $\dot{r}$ are the signal envelope and its derivative, respectively. The LCR crossing in the negative direction can be calculated by the same integral with the range of $(-\infty, 0)$. The results should be the same. Following the definition, the proposed FR-LCR can be obtained as

$$\lambda_R = f(r_s = R)\int_0^\infty \dot{r}_s f(\dot{r}_s)d\dot{r}_s = \frac{\sigma_{\dot{r}_s}}{\sqrt{2\pi}} f(r_s = R). \tag{21}$$

By plugging (14) and (19) into (21), we can obtain

$$\lambda_R = \frac{\sigma_{\dot{x}\dot{y}}}{\sqrt{\pi}\Gamma(m)}\left(\frac{m}{\Omega_s}\right)^m R^{2m-1}\exp\left(-\frac{m}{\Omega_s}R^2\right) \tag{22}$$

where $\sigma_{\dot{x}\dot{y}}$ is given in (17), and Ω_s is the average power of a subchannel, as given in (8). As shown, $\sigma_{\dot{x}\dot{y}}$ is proportional to the RMS delay τ_{RMS} of the CIR of the wideband operator channel. A larger delay spread results in a higher LCR in the frequency domain, i.e., more severe fluctuation in the frequency response, and vice versa. In addition, the authors in [13] predicted that FD-LCR should be proportional to τ_{RMS} and we have obtained the same result in (22).

Furthermore, we are interested in the correlation of the received power of the subchannels, which depends on the variation of the PSD of the wideband channel. The PSD-LCR at threshold W is obtained by substituting R by $\sqrt{W}$ in (22), which is

$$\Lambda_W = \frac{\sigma_{\dot{x}\dot{y}}}{\sqrt{\pi}\Gamma(m)}\left(\frac{m}{\Omega_s}\right)^m W^{m-\frac{1}{2}}\exp\left(-\frac{m}{\Omega_s}W\right). \tag{23}$$

VII. Finite-State Markov Chain and Subchannel Small-Scale Fading Correlation

A. *FSMC in Frequency Domain*

As discussed in Section II-A, FSMC has been widely adopted to describe the temporal fading of a wireless channel. Based on this idea, we construct a first-order FSMC to model the received power variation of different subchannels.

First, we partition the received power range into K nonoverlapping intervals, which are defined as the K states of the subchannels. Let $\mathbb{S} = S_1, S_2, \ldots, S_K$ denote the subchannel power state space where S_k corresponds to the kth power interval of (W_k, W_{k+1}). The granularity of the power interval should be elaborately designed to satisfy the following two requirements. First, the PSD associated with one subchannel remains in the same interval and, when there happens to be a subchannel handover (i.e., frequency increases from one subchannel to the next), the PSD may either stay in the same interval or only transit into adjacent interval(s). This condition can be satisfied because the subchannel bandwidth is much smaller than the channel coherence bandwidth; thus, the PSD cannot change significantly. Second, the power range should not be too large to ensure that the received power within one interval is similar.

Theoretically speaking, the received power spans from 0 to ∞. Following the equal probability method (EPM) [5], we limit the partition such that the steady-state probability of each state, which is denoted $\pi_k (k = 1, 2, \ldots, K)$, is the same as $1/K$. As a consequence, the thresholds W_k satisfy the condition of

$$\pi_k = \int_{W_k}^{W_{k+1}} f_{w_s}(w)dw = F_{w_s}(W_{k+1}) - F_{w_s}(W_k) = \frac{1}{K} \tag{24}$$

where $k = 1, 2, \ldots, K$, $F_{w_s}(w)$ is the cumulative distribution function (cdf) of the received power of a subchannel, $W_1 = 0$, and $W_{K+1} = \infty$.

Since the received signal envelop of one subchannel has Nakagami-m fading, the received power $w_s = r_s^2$ is Gamma distributed [5] and

$$F_{w_s}(w) = \frac{1}{\Gamma(m)}\gamma\left(m, \frac{m}{\Omega_s}w\right) \tag{25}$$

where $\gamma(\cdot)$ is the incomplete gamma function. By plugging (25) into (24) and numerically solving the equation set, the thresholds W_k $(k = 2, 3, \ldots, K)$ can be obtained.

By appropriately choosing the granularity, it can be guaranteed that the state transitions occur almost only between adjacent states in the proposed Markov model. Let $t_{i,j}$ denote the transition probability from state S_i of one subchannel to S_j of the next subchannel, and $t_{i,j}$ can be approximated by

$$\begin{cases} t_{k,k-1} \approx \frac{B_s N(W_k)}{U_f \pi_k}, & k = 2, 3, \ldots, K \\ t_{k,k+1} \approx \frac{B_s N(W_{k+1})}{U_f \pi_k}, & k = 1, 2, \ldots, K-1. \end{cases} \tag{26}$$

In (26), U_f/B_s is the number of subchannels within the unit bandwidth, and $U_f \pi_k / B_s$ is the average number of subchannels with the received power in state S_k. Equation (26) is the ratio of the expected number of times the PSD crossing the threshold W_k within U_f to the average number of subchannels staying in S_k within U_f. Therefore, (26) gives the probability of crossing the threshold of W_k (i.e., moving into the state S_{k-1}) given that the current state is S_k, which is the state transition probability $t_{k,k-1}$. $t_{k,k+1}$ is derived based on the same idea. The remaining self-transition probabilities are obtained by

$$t_{k,k} = \begin{cases} 1 - t_{1,2}, & k = 1 \\ 1 - t_{K,K-1}, & k = K \\ 1 - t_{k,k-1} - t_{k,k+1}, & k = 2, \ldots, K-1. \end{cases} \tag{27}$$

B. Correlation of Subchannel SSF

The proposed FSMC can guarantee the Nakagami-m distribution of the subchannels and the correlation between them. We can evaluate empirically the CCC between the subchannels by the generated state samples. Suppose that $\mathbf{S}$ is the subchannel state sequence within the operator channel spectrum generated by the proposed FSMC model. $\mathbf{S}_l = S^{(l)}, S^{(l+1)}, \ldots, S^{(l+m)}, \ldots$ is the sequence beginning from the lth subchannel, where $S^{(l+m)}$ is the state of the $(l+m)$th subchannel. The CCC of two subchannels separated by L subchannels can be calculated by

$$\rho_L = \frac{\mathrm{cov}(\mathbf{S}_1, \mathbf{S}_{1+L})}{\sqrt{\mathrm{var}(\mathbf{S}_1)\mathrm{var}(\mathbf{S}_{1+L})}}. \tag{28}$$

In addition, the numerical results indicate that ρ_L may be negative due to the mathematical modeling. Therefore, we add a boundary for the CCC such that it is guaranteed to be larger than or equal to zero. Thus, the simulation result is

$$\rho'_L = \max\{0, \rho_L\}. \tag{29}$$

VIII. Model Evaluation

As an example, the parameters of a CA system are as follows. The spectrum of the operator channel is 2–3 GHz.

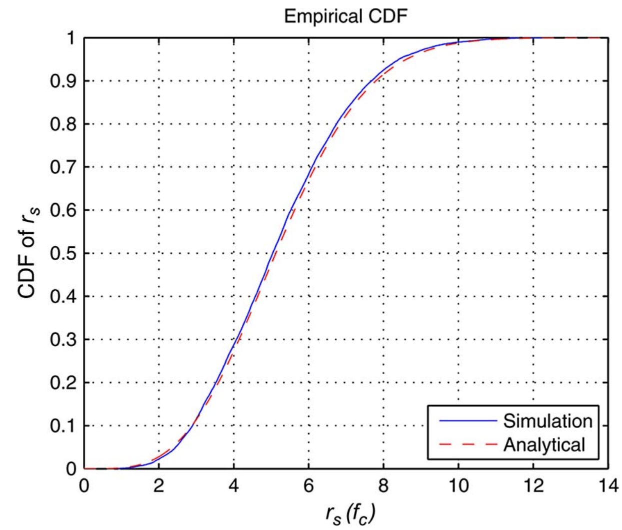

Fig. 9. CDF of the subchannel envelop generated by the propagation model.

In a static multipath environment, the PDP of the operator channel is exponentially decaying with $\tau_{\mathrm{RMS}} = 300$ ns, and the maximal power of the MPCs is $A = 1$ unit. We set the threshold coefficient $\alpha = 0.1$ for the received power of a valid MPC, i.e., 10-dB power attenuation compared with the largest MPC. The corresponding maximal excess delay of the valid MPCs is $\tau_M = 690.8$ ns. Suppose that there are $N = 40$ valid paths. To evaluate the variation of the wideband channel PSD by a fine granularity, the subchannel bandwidth is assumed 40 kHz. The Nakagami-m fading parameter of the subchannels is $m = 2$.

A. Propagation Model

The propagation model proposed in (13) is simulated to generate the channel gain (i.e., the envelop of the received signal) of the $2.5 * 10^4$ subchannels inside the 1-GHz operator spectrum. Fig. 9 shows the empirical cdf of the channel gain of the subchannels. The theoretical cdf of Nakagami-m fading is also plotted with the average power of $\Omega_s = 31.27$ calculated by (15). It can be seen that the channel gain generated by the proposed propagation model has exactly the Nakagami-m distribution with the estimated parameters.

B. PSD-LCR in Frequency Domain

The PSD can be obtained by $w_s = r_s^2$, where r_s is the channel gain of the subchannels generated by the propagation model. The simulated LCR is acquired by counting the level crossing of the generated PSD within the bandwidth from 2 to 3 GHz and by calculating the average times for the unit bandwidth of $U_f = 100$ MHz. Fig. 10 compares the simulation results and the theoretical results from (23). The 15 thresholds are chosen such that the PSD would fit into each interval with equal probability according to the EPM.

Although [15, Fig. 1] and our results in Fig. 10 show the FD-LCR for frequency-selective Rayleigh and Nakagami-m fading, respectively, the trend of the results are consistent: higher for the thresholds in the middle range and lower for the small and large thresholds.

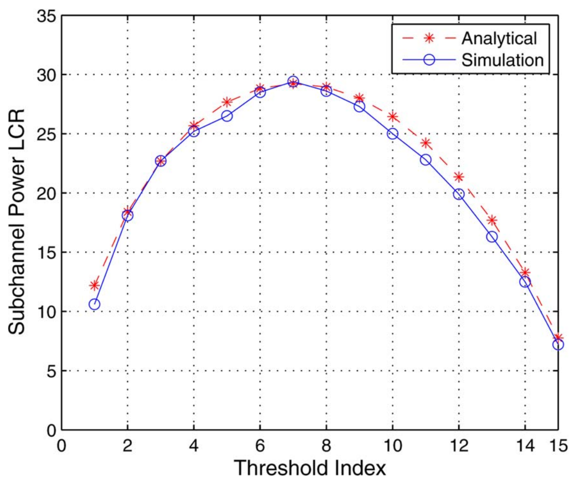

Fig. 10. Frequency-domain LCR of the subchannel received power.

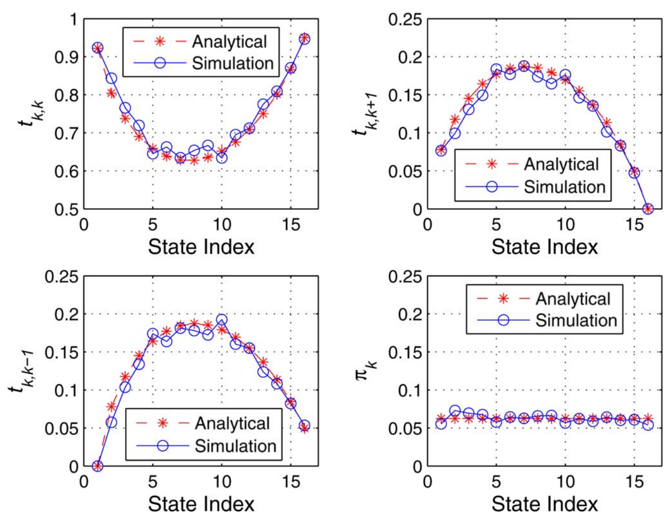

Fig. 11. Transition probabilities and steady-state probabilities of the FSMC.

C. Frequency-Domain FSMC

Using the same 15 thresholds as earlier, we establish a 16-state FSMC model for the received power variation among the subchannels. For the transition probabilities $t_{i,j}$ and the steady-state probabilities π_k, the simulation results obtained from the generated subchannel power sequence and the analytical results calculated by (26) and (27), are compared in Fig. 11. The agreement between the results has verified that the FSMC can preserve the statistical properties and the correlation of the subchannel power values.

D. Subchannel Correlation

The correlation coefficient of two subchannels separated by various frequency bandwidth is calculated according to (28) and shown in Fig. 12. The autoregression result with the sliding window size of 800 kHz is also plotted. As shown, in a propagation environment with an intensive multipath effect and exponentially decaying PDP (with $\tau_{\rm RMS} = 300$ ns), the correlation coefficient is above 0.5 when the gap of two subchannels is smaller than 5 MHz, and they are almost uncorrelated when the frequency gap is larger than 50 MHz.

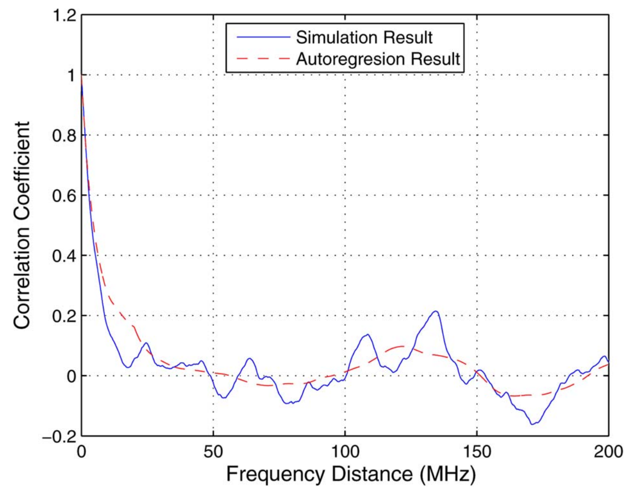

Fig. 12. Correlation coefficient of the subchannel received power.

E. Comparison of Measurement, Simulation, and Analytical Results

The CCC of subchannel SSF obtained by the measurement, the proposed FSMC model, and the analytical results are compared for two regions, $F1$ and E, which are typical for LOS and NLOS scenarios, respectively. The RMS delay spread of the SSA-PSD of $F1$ and E are $\tau_{\rm RMS} \approx 14.9$ ns and $\tau_{\rm RMS} \approx 39.8$ ns, respectively, based on measurement, as shown in Fig. 3. We establish two FSMC models according to $\tau_{\rm RMS}$. The simulation CCC of two subchannels when they are separated by 0–200 MHz is calculated by (29) and analytical results by (1). Because we focus on the fading process between the subchannels at one time instant, we have $m_1 = m_2$ and $\tau = 0$. Furthermore, the numerical experiment has shown that the closed-form approximation expression in (1) is quite accurate compared with the exact expression. Therefore, similar to [3, Sec. IV-A], we adopt the approximation, and the CCC is calculated by $\rho(\Delta\omega) = (1/1 + (\Delta\omega\bar{T})^2)$, where the frequency separation is $\Delta\omega \in [0 \sim 200 \times 10^6] \times 2\pi$ rad/s. Based on the measurement results, the mean excess delay $\bar{T}$ is 6.7 and 30.4 for region $F1$ and E, respectively. The measurement, simulation, and analytical results are plotted in Fig. 13.

Fig. 13 shows that the subchannels are more correlated in the LOS scenario. This is expected as smaller $\tau_{\rm RMS}$ leads to a larger coherence bandwidth and, thus, a higher CCC between the subchannels. Furthermore, the CCC in [13, Fig. 6] has an exponentially decaying pattern with the increase in frequency spacing, the same as the results in Figs. 12 and 13.

The results of the measurement, FSMC simulation, and analysis match each other reasonably in the LOS scenario. In the NLOS scenario, the difference is more obvious. It is likely because the presented results are based on a specific set of measurements made within an office building. It has been noted that the building architecture has a significant effect on the fading profile of the channel [22], [25]. In the NLOS scenario, the effect of the building on the channel response may be more significant, leading to more randomness in the measurement result. For example, Fig. 13 shows that the correlation in the measurement does not decay as fast as predicted by the analytical model. This may be due to the following

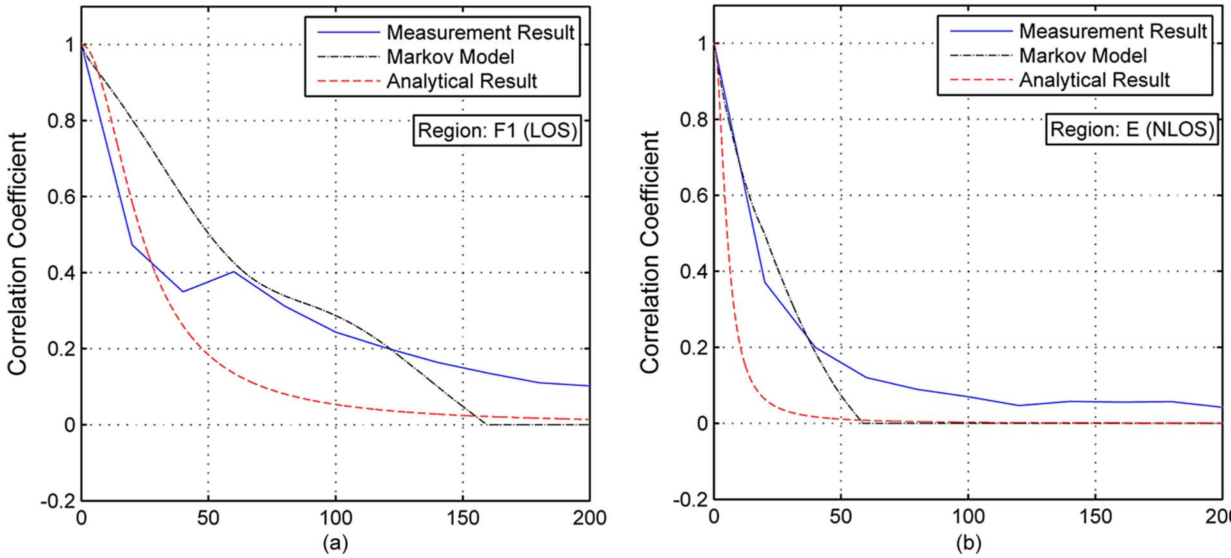

Fig. 13. Comparison of subchannel CCC for region $F1$ and E.

reason. In this particular experimental environment, a few of the paths with excess delay are much smaller than the mean delay and contribute to a high percentage of the overall received energy, which results in the nonzero correlation over a larger bandwidth gap. Therefore, collection of more propagation data from different buildings and outdoor environments are needed to determine the typical CCF between subchannels.

IX. Conclusion

In this paper, the spatial correlation of subchannels has been quantified based on both measurement and FSMC modeling. The UWB measurement approach provides a feasible way to evaluate the fading of separated subchannels. The FSMC based on the typical exponentially decaying PDP of wideband channels provides a fast way to simulate the frequency-selective fading between the subchannels. The measurement and simulation results are compared with the analytical results. It is found that the LSF of a single subchannel is environment specific, resulting in low autocorrelation. However, the LSF of even well separated subchannels is fully correlated due to identical shadowing effect. The minimal frequency spacing of two uncorrelated subchannels varies from 40 to over 100 MHz, depending on the LOS or NLOS scenario. The SSF of two subchannels is almost uncorrelated if they are separated by nearly 100 MHz, probably because of the intensive multipath effect. In the time domain, the correlation coefficient of the PDPs is above 0.8 in the LOS scenario when the receiver moves within a distance of about 10λ, which means the multipath profile varies slightly. However, PDP changes faster and more significantly in the NLOS scenario, particularly when the SNR is low. The main contributions of this paper are in the development of the measurement approach and the Markovian modeling on frequency-selective fading.

This paper has suggested that more propagation data are needed to determine whether the results presented here are typical. Furthermore, the results obtained in this paper help with the design of subchannel estimation/combination strategies by taking the correlation properties into account. For example, if the subchannel between a BS and user equipment (UE) has a high channel gain, it is quite likely that it can successfully increase the throughput to the UE by aggregating another subchannel due to the high LSF correlation. The frequency band to aggregate can be selected depending on the spectrum availability and it does not necessarily need to be adjacent. Thus, bandwidth-demanding applications, such as video streaming, can be supported. As another example, since the SSF correlation between two subchannels turns out to be low if the frequency spacing is beyond 100 MHz, the channel estimation overhead cannot be significantly reduced. If the spacing is small (such as less than 40 MHz), the channel estimation may be avoided or simplified, particularly in the LOS case due to the high correlation. However, if two subchannels separated by more than 100 MHz are aggregated, frequency diversity may be exploited. The coverage analysis of CA may consider the full correlation of the LSF of the subchannels, even if they are well separated.

References

[1] K. Pedersen *et al.*, "Carrier aggregation for LTE-advanced: Functionality and performance aspects," *IEEE Commun. Mag.*, vol. 49, no. 6, pp. 89–95, Jun. 2011.

[2] J. Cai, X. Shen, J. Mark, H. Liu, and T. Todd, "Semiblind channel estimation for pulse-based ultra-wideband wireless communication systems," *IEEE Trans. Veh. Technol.*, vol. 55, no. 1, pp. 95–103, Jan. 2006.

[3] J. S. Filho, G. Fraidenraich, U. Dias, and M. Yacoub, "On the Nakagami-m crosscorrelation function," in *Proc. SBMO/IEEE MTT-S Int. Conf. Microw. Optoelectron.*, Jul. 2005, pp. 513–516.

[4] "Requirements for Further Advancements for Evolved Universal Terrestrial Radio Access (E-UTRA)," Sophia-Antipolis, France, Std. 3GPP TR 36.913, version 8.0.1, Mar. 2009.

[5] C. Iskander and P. T. Mathiopoulos, "Fast simulation of diversity Nakagami fading channels using finite-state Markov models," *IEEE Trans. Broadcast.*, vol. 49, no. 3, pp. 269–277, Sep. 2003.

[6] "Winner II channel models," Munich, Germany, Tech. Rep. IST-4-027756 WINNER II, D.1.1.2 V1.2, Sep. 2007.

[7] P. Zetterberg, N. Jalden, K. Yu, and M. Bengtsson, "Analysis of MIMO multi-cell correlations and other propagation issues based on urban measurements," in *Proc. IST Mobile Summit*, Jun. 2005, pp. 1–5.

[8] A. Hong *et al.*, "Experimental evaluation of correlation properties of large scale parameters in an indoor LOS environment," in *Proc. 3rd ISWCS*, Valencia, Spain, Sep. 2006, pp. 55–59.

[9] N. Jalden, P. Zetterberg, B. Ottersten, A. Hong, and R. Thoma, "Correlation properties of large scale fading based on indoor measurements," in *Proc. IEEE WCNC*, Mar. 2007, pp. 1894–1899.

[10] J. Filho, M. Yacoub, and G. Fraidenraich, "A simple accurate method for generating autocorrelated Nakagami-m envelope sequences," *IEEE Commun. Lett.*, vol. 11, no. 3, pp. 231–233, Mar. 2007.

[11] C.-D. Iskander and P. Mathiopoulos, "Analytical envelope correlation and spectrum of maximal-ratio combined fading signals," *IEEE Trans. Veh. Technol.*, vol. 54, no. 1, pp. 399–404, Jan. 2005.

[12] H. S. Wang and N. Moayeri, "Finite-state Markov channel: A useful model for radio communication channels," *IEEE Trans. Veh. Technol.*, vol. 44, no. 1, pp. 163–171, Feb. 1995.

[13] K. Witrisal, Y. Kim, and R. Prasad, "Frequency-domain simulation and analysis of the frequency-selective Ricean fading radio channel," in *Proc. IEEE PIMRC*, Sep. 1998, pp. 1131–1135.

[14] R. Zhang and L. Cai, "Packet-level channel model for wireless OFDM systems," in *Proc. IEEE GLOBECOM*, Nov. 2007, pp. 5215–5219.

[15] F. Lopez-Martinez, E. Martos-Naya, J. F. Paris, and U. Fernandez-Plazaola, "Higher order statistics of sampled fading channels with applications," *IEEE Trans. Veh. Technol.*, vol. 61, no. 7, pp. 3342–3346, Sep. 2012.

[16] M. Win, R. Scholtz, and M. Barnes, "Ultra-wide bandwidth signal propagation for indoor wireless communications," in *Proc. IEEE ICC*, Jun. 1997, pp. 56–60.

[17] D. Cassioli, M. Win, and A. Molisch, "The ultra-wide bandwidth indoor channel: From statistical model to simulations," *IEEE J. Sel. Areas Commun.*, vol. 20, no. 6, pp. 1247–1257, Aug. 2002.

[18] H. Schantz and L. Fullerton, "The diamond dipole: A Gaussian impulse antenna," in *Proc. IEEE Antennas Propag. Soc. Int. Symp.*, Jul. 2001, pp. 100–103.

[19] R. Zhang, Y. Zhang, Z. Zhong, and X. Lu, "The correlation properties of subchannel fading for non-continuous carrier aggregation based on indoor ultra-wideband measurement," in *Proc. IEEE GLOBECOM*, Dec. 2012, pp. 4071–4077.

[20] Y. Wang and N. Zhang, "A new multi-template CLEAN algorithm for UWB channel impulse response characterization," in *Proc. ICCT*, Nov. 2006, pp. 1–4.

[21] J. A. Hogbom, "Aperture synthesis with a nonregular distribution of interferometer baselines," *Astron. Astrophys. Suppl. Ser.*, vol. 15, pp. 417–426, Jun. 1974.

[22] R. Cramer, R. Scholtz, and M. Win, "Evaluation of an ultra-wide-band propagation channel," *IEEE Trans. Antennas Propag.*, vol. 50, no. 5, pp. 561–570, May 2002.

[23] R. Valenzuela, O. Landron, and D. Jacobs, "Estimating local mean signal strength of indoor multipath propagation," *IEEE Trans. Veh. Technol.*, vol. 46, no. 1, pp. 203–212, Feb. 1997.

[24] M. D. Yacoub, J. E. V. Bautista, and L. Guerra de R. Guedes, "On higher order statistics of the Nakagami-m distribution," *IEEE Trans. Veh. Technol.*, vol. 48, no. 3, pp. 790–794, May 1999.

[25] Q. Spencer, B. Jeffs, M. Jensen, and A. Swindlehurst, "Modeling the statistical time and angle of arrival characteristics of an indoor multipath channel," *IEEE J. Sel. Areas Commun.*, vol. 18, no. 3, pp. 347–360, Mar. 2000.

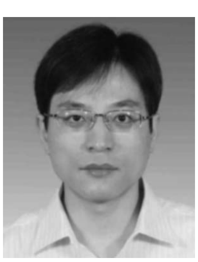

Ruonan Zhang (S'09–M'11) received the B.S. and M.S. degrees from Xi'an Jiaotong University, Xi'an, China, in 2000 and 2003, respectively, and the Ph.D. degree from the University of Victoria, BC, Canada, in 2010.

From 2003 to 2006, he was with Motorola Inc. and then with Freescale Semiconductor Inc., Tianjin, China, working on integrated-circuit architecture and application system design. He is currently an Associate Professor with the School of Electronics and Information, Northwestern Polytechnical University, Xi'an. His current research interests include wireless channel measurement and modeling, architecture and protocol design of wireless networks, cooperative networking, and satellite communications.

Zhimeng Zhong received the B.Sc., M.Sc., and Ph.D. degrees from Xi'an Jiaotong University, Xi'an, China, in 2002, 2005, and 2008, respectively, all in electronic engineering.

He is currently an Algorithm Engineer with Huawei Technologies Ltd., Xi'an. His current research interests include digital wireless communications, wireless channel measurement and modeling, distributed space–time coding, cooperative communications, and multiple-input–multiple-output systems.

Yang Zhang received the Ph.D. degree in electrical engineering from Xidian University, Xi'an, China, in 2011.

From 2009 to 2010, he was a Visiting Scholar with the Department of Electrical and Computer Engineering, University of California, Davis, CA, USA. After working with Huawei Technologies from 2011 to 2013, he rejoined Xidian University. His main research interests include cooperative communications, resource-allocation strategies, network lifetime optimization, and wireless channel modeling.

Stan (Xiaofeng) Lu received the B.S. degree in electronic engineering from the University of Electronic Science and Technology of China, Chengdu, China, and the M.S. degree in automatic control from Lanzhou University, Lanzhou, China, in 1993 and 2000, respectively. He received the Ph.D. degree from Xi'an Jiaotong University, Xi'an, China, in 2003.

From 2003 to 2008, he was with ZTE Corporation and, from 2008 to 2014, with Huawei Technologies. His main research interests include wireless channel modeling, machine learning, and pattern recognition.

Lin Cai (S'00–M'06–SM'10) received the M.A.Sc. and Ph.D. degrees in electrical and computer engineering from the University of Waterloo, ON, Canada, in 2002 and 2005, respectively.

Since 2005, she has been an Assistant Professor and then an Associate Professor with the Department of Electrical and Computer Engineering, University of Victoria, BC, Canada. Her research interests include wireless communications and networking, with a focus on network protocol and architecture design supporting emerging multimedia traffic over wireless, mobile, ad hoc, and sensor networks.

Dr. Cai received an Outstanding Achievement in Graduate Studies Award.